



Bimodular architecture of bacterial effector SAP05 that drives ubiquitin-independent targeted protein degradation

Qun Liu^{a,1} , Abbas Maqbool^{b,c,1} , Federico G. Mirkin^a , Yeshveer Singh^a , Clare E. M. Stevenson^b , David M. Lawson^b , Sophien Kamoun^c , Weijie Huang^{d,2} , and Saskia A. Hogenhout^{a,2}

Edited by Ning Zheng, University of Washington, Seattle, WA; received June 26, 2023; accepted October 19, 2023 by

Editorial Board Member Sheng Yang He

In eukaryotes, targeted protein degradation (TPD) typically depends on a series of interactions among ubiquitin ligases that transfer ubiquitin molecules to substrates leading to degradation by the 26S proteasome. We previously identified that the bacterial effector protein SAP05 mediates ubiquitin-independent TPD. SAP05 forms a ternary complex via interactions with the von Willebrand Factor Type A (vWA) domain of the proteasomal ubiquitin receptor Rpn10 and the zinc-finger (ZnF) domains of the SQUAMOSA-PROMOTER BINDING PROTEIN-LIKE (SPL) and GATA BINDING FACTOR (GATA) transcription factors (TFs). This leads to direct TPD of the TFs by the 26S proteasome. Here, we report the crystal structures of the SAP05–Rpn10^{vWA} complex at 2.17 Å resolution and of the SAP05–SPL5^{ZnF} complex at 2.20 Å resolution. Structural analyses revealed that SAP05 displays a remarkable bimodular architecture with two distinct nonoverlapping surfaces, a “loop surface” with three protruding loops that form electrostatic interactions with ZnF, and a “sheet surface” featuring two β-sheets, loops, and α-helices that establish polar interactions with vWA. SAP05 binding to ZnF TFs involves single amino acids responsible for multiple contacts, while SAP05 binding to vWA is more stable due to the necessity of multiple mutations to break the interaction. In addition, positioning of the SAP05 complex on the 26S proteasome points to a mechanism of protein degradation. Collectively, our findings demonstrate how a small bacterial bimodular protein can bypass the canonical ubiquitin–proteasome proteolysis pathway, enabling ubiquitin-independent TPD in eukaryotic cells. This knowledge holds significant potential for the creation of TPD technologies.

targeted protein degradation | ubiquitin-independent | bacterial effector protein | 26S proteasome | phytoplasma

Pathogenic bacteria secrete effector proteins that manipulate host cell processes, aiding in bacterial survival and often resulting in disease (1). These effector proteins are a source of biochemical innovation and include some of the most remarkable proteins known to function inside host cells. Notable examples include Transcription Activator-Like (TAL) effectors, derived from plant pathogenic bacteria, which can be engineered to bind specific DNA sequences (2), type-III effector proteins from animal parasitic bacteria, capable of re-engineering kinase pathways (3), and the CRISPR/Cas systems—immune defenses against bacteriophages, now harnessed as groundbreaking genetic manipulation tools (4). In addition, we recently identified that SAP05 effectors of bacterial phytoplasma pathogens enable the degradation of structured proteins by the 26S proteasome in a ubiquitin-independent manner (5). Similar to other bacterial effectors, the utility of SAP05 proteins can extend beyond the realm of natural biology, as they have the potential to serve as tools in biotechnology and biomedicine. However, unraveling the structure–function relationships and underlying mechanisms of SAP05 bacterial effectors is necessary to pave the way for their applications in synthetic biology.

Efficient and selective protein degradation is crucial for all living organisms (6, 7). A significant portion of energy in cells is devoted to the process of protein degradation. This expenditure of energy is vital for cells to adapt and react to their surrounding environment (8–13). Protein degradation is executed by a diverse family of enzymes, proteases, that hydrolyse peptide bonds (6). To prevent the destruction of proteins not destined for degradation and avoid the accidental disruption of the cellular proteome, protein degradation must be spatially and temporally controlled (14–16).

The 26S proteasome is such a self-compartmentalizing device. It is a highly sophisticated complex with distinct proteolytic activities able to degrade proteins selectively and efficiently in all eukaryotes (14, 17). With 33 different subunits and approximately 2.5 MDa in mass, it is the largest ATP-dependent protease machinery in the cell (16, 18, 19). The subunits are organized in two particles: the catalytic 20S core particle (CP) and the 19S regulatory particle (RP). The 20S CP is a cylindrical complex containing four heptameric rings with

Significance

This study reveals the structure–function relationships and mechanisms of SAP05 bacterial effectors in a unique protein degradation process. Crystal structures demonstrate that SAP05 acts as a scaffold, facilitating efficient substrate degradation by bringing together the substrate and the 26S proteasome receptor Rpn10. Substrate degradation triggered by direct interaction of SAP05 and a specific 26S proteasome component is independent of ubiquitination, distinct from PROteolysis-TArgeting Chimeras (PROTAC) and other similar systems. This finding can guide the design of SAP05-like molecules for a protein degradation technology with significant potential in biotechnology and biomedicine. It also emphasizes the capacity of proteasome subunits to initiate protein degradation, promoting the advancement of alternative approaches that bypass ubiquitination.

Preprint Server: <https://www.biorxiv.org/content/10.1101/2023.06.19.545293v1>. The copyright holder for this preprint is the author/funder, who has granted bioRxiv a license to display the preprint in perpetuity. It is made available under a CC-BY 4.0 International license.

This article is a PNAS Direct Submission. N.Z. is a guest editor invited by the Editorial Board.

Copyright © 2023 the Author(s). Published by PNAS. This open access article is distributed under [Creative Commons Attribution License 4.0 \(CC BY\)](https://creativecommons.org/licenses/by/4.0/).

¹Q.L. and A.M. contributed equally to this work.

²To whom correspondence may be addressed. Email: wjhuang@cemps.ac.cn or saskia.hogenhout@jic.ac.uk.

This article contains supporting information online at <https://www.pnas.org/lookup/suppl/doi:10.1073/pnas.2310664120/-/DCSupplemental>.

Published December 1, 2023.

multiple catalytic β subunits and can degrade intrinsically disordered proteins by itself, including proteins that are unfolded by damage or mutations (20, 21). The 19S regulatory particle (RP) sits on one or both sides of the CP and is primarily required for the degradation of structured proteins via mechanically translocating substrates into the degradation chamber of the CP.

The degradation of structured proteins in eukaryotic organisms is predominantly regulated by the ubiquitin–proteasome system (UPS) (22, 23). UPS involves prior decoration of substrates with ubiquitin chains via the complex and consecutive actions of E1, E2, and E3 ligase enzymes (20, 24–27). The ubiquitin chains are recognized by 19S RP substrate receptors regulatory particle non-ATPase (Rpn) 1, Rpn10, and Rpn13, which enable substrate degradation by translocating stretched unstructured regions into the 20S CP channel (7, 17). Efficient degradation is also dependent on Rpn11 that removes the ubiquitin units during substrate translocation (8, 15). Beyond binding ubiquitinated substrates, the multimodular Rpn1, Rpn10, and Rpn13 enable transient interactions with ubiquitin-binding shuttle factors, such as RADIATION-SENSITIVE PROTEIN 23 (RAD23), and ubiquitin processing enzymes (7, 12).

A number of bacterial effector proteins target or co-opt the UPS. Among these, SAP05 effectors of bacterial phytoplasma pathogens enable the degradation of structured proteins by the 26S proteasome in a ubiquitin-independent manner (5). SAP05 binds both the von Willibrand factor type A (vWA) domain of Rpn10 and the zinc-finger (ZnF) domain of multiple members of two distinct plant transcription factor families, known as SQUAMOSA-PROMOTER BINDING PROTEIN-LIKE (SPL) and GATA BINDING FACTORS (GATAs) (5). By hijacking Rpn10, SAP05 mediates the degradation of these TFs, leading to dramatic changes in plant development that includes leaf and stem proliferations, neoteny and increased longevity (5), as well as increased plant colonization of phytoplasma insect vectors (28). Other phytoplasma effectors, known as SAP54/phylogenins, were found to hijack the 26S proteasome shuttle factor RAD23 to mediate the degradation of plant MCM1, AGAMOUS, DEFICIENS, and SRF (MADS) domain transcription factors leading to the induction of leaf-like flowers and other changes in flower development (29), and this also occurs in a ubiquitin-independent manner (30). Therefore, phytoplasma effectors appear to directly target ubiquitin receptors or shuttle factors to mediate ubiquitin-independent protein degradation. However, the precise biochemical mechanisms by which these small effector proteins form connections between unrelated proteins to mediate targeted protein degradation in a ubiquitin-independent manner remain uncharacterized.

Here, we determined how SAP05 mediates ubiquitin-independent targeted protein degradation by generating crystal structures of SAP05 in complex with the ZnF domain of SPL5 (SPL5^{ZnF}) and with the vWA domain of Rpn10 (Rpn10^{vWA}) and validating the ensuing mechanistic model using mutagenesis and protein degradation experiments. We found that SAP05 acts like a scaffold by bridging ZnF and vWA on opposing surfaces at 1:1 stoichiometries. Furthermore, SAP05 binding to vWA does not appear to cause steric hindrance with other 26S proteasome components and their interactors. Our data show how the bacterial SAP05 effector has evolved as a functional adapter of the 26S proteasome to bypass the canonical UPS cellular proteolysis pathway and enable ubiquitin-independent degradation of structured eukaryotic proteins.

Results

Crystal Structures of the SAP05–SPL5^{ZnF} and SAP05–Rpn10^{vWA} Complexes Reveal Two Distinct Binding Faces of SAP05. We previously demonstrated that SAP05 of Aster Yellows phytoplasma

strain Witches Broom (AYWB) forms a ternary complex with the ZnF domain of SPL5 (SPL5^{ZnF}) and vWA domain of Rpn10 (Rpn10^{vWA}) (5). To investigate how SAP05 binds these two larger proteins, we determined crystal structures of SAP05 in complex with SPL5^{ZnF} and with Rpn10^{vWA}. We expressed constructs containing SAP05 residues 33 to 135 that correspond to the entire mature part of SAP05 (without the first 32 amino acids encoding the signal peptide that is cleaved off during secretion of the effector), residues 60 to 127 of *Arabidopsis thaliana* SPL5 (accession number AT3G15270) corresponding to the ZnF domain and residues 2 to 193 comprising the vWA domain of *A. thaliana* Rpn10 (accession number AT4G38630) (SI Appendix, Fig. S1A) in *Escherichia coli*. SAP05 and SPL5^{ZnF} were individually expressed and successfully purified at high purity with immobilized metal-affinity chromatography (IMAC) via 6 \times His tags followed by tag removal and gel filtration (Superdex 75 26/60) (SI Appendix, Fig. S1B). As Rpn10^{vWA} formed aggregates upon purification in the absence of SAP05, Rpn10^{vWA} was coexpressed with SAP05 and purified as a complex using the same general method (SI Appendix, Fig. S1B). To generate the SAP05–SPL5^{ZnF} complex, we mixed equimolar amounts of purified SAP05 and SPL5^{ZnF}.

We obtained crystals for both complexes, which yielded X-ray data to 2.20 Å resolution for SAP05–SPL5^{ZnF} and to 2.17 Å resolution for SAP05–Rpn10^{vWA}. The structure of the SAP05–SPL5^{ZnF} complex was solved via the single-wavelength anomalous diffraction method due to the presence of Zn²⁺ ions bound to ZnF, and that of SAP05–Rpn10^{vWA} was solved with the molecular replacement method using a copy of SAP05 from the SAP05–SPL5^{ZnF} structure and a homology model for Rpn10^{vWA} as templates. The details of X-ray data processing and structure solution are described in *Materials and Methods*. The X-ray data collection, refinement, and validation statistics are shown in Table 1.

The structure of SPL5^{ZnF} resembles the previously determined NMR structures of ZnF domain of *A. thaliana* SPL4 (PDB 1UL4; rmsd = 1.56 Å) and SPL7 (PDB 1UL5; rmsd = 1.76 Å) (31). As well, our Rpn10^{vWA} structure is similar to that of vWA in the spinach 26S proteasome Cryo-EM structure (PDB 8AMZ; rmsd = 0.91 Å) (32). However, a search for SAP05 structure homologues using DALI sever (<http://ekhidna2.biocenter.helsinki.fi/dali/>) (33) and PDBeFold server (<https://www.ebi.ac.uk/msd-srv/ssm/>) (34) failed to identify any publicly available, experimentally determined structures with significant structural similarity to SAP05.

The SAP05 protein comprises a globular compact structure with five β -strands that form an internal triangular mixed β -sheet core (Fig. 1A and B). β -strand 1 (β 1) locates on the long end of this triangular core and connects via a loop–helix–loop–helix–loop structure to β 2 at the opposite surface near the tip of this core. This β -strand is connected to β 3 and β 4 via loop structures that form the loop-dominated surface of the protein. β 4 then connects to a loop–helix–loop structure that runs back to near the long end of the core to β 5, which runs parallel to β 1 (Fig. 1A). Both the SAP05–SPL5^{ZnF} and SAP05–Rpn10^{vWA} structures comprise a 1:1 complex (Fig. 1C and D). The SAP05 residues binding ZnF and vWA are located at opposing surfaces of the effector with the ZnF binding surface comprising the loop-dominated surface (loop surface) and the vWA-binding surface the β -sheet-dominated long end of the triangular β -sheet core (sheet surface) (Fig. 1B and E).

We were able to assemble the ternary complex containing ZnF, SAP05 and vWA by mixing equimolar amounts of the purified SAP05–Rpn10^{vWA} complex and purified SPL5^{ZnF} followed by gel filtration (Fig. 1F and SI Appendix, Fig. S1B), as shown previously (5). Therefore, SAP05 has the capacity to bind ZnF and vWA simultaneously to form a ternary complex (Fig. 1G). The SAP05 structures are essentially the same between the SAP05–SPL5^{ZnF}

Table 1. X-ray data collection, processing, and refinement statistics

Dataset	SAP05–SPL5 ^{ZnF} SAD phasing	SAP05–SPL5 ^{ZnF} refinement	SAP05–Rpn10 ^{vWA}
Data collection			
Diamond light source beamline	I04	I04	I04
Wavelength (Å)	1.2770	0.9795	0.9796
Detector	Eiger2 XE 16 M	Eiger2 XE 16 M	Eiger2 XE 16 M
Resolution range (Å)	70.27–2.90 (3.08–2.90)	82.51–2.20 (2.24–2.20)	68.60–2.17 (2.24–2.17)
Space group	<i>P</i> 2 ₁	<i>P</i> 2 ₁	<i>P</i> 2 ₁
Cell parameters (Å/°)	<i>a</i> = 78.87, <i>b</i> = 165.33, <i>c</i> = 80.99, β = 109.62	<i>a</i> = 78.69, <i>b</i> = 165.02, <i>c</i> = 80.86, β = 109.65	<i>a</i> = 42.39, <i>b</i> = 68.60, <i>c</i> = 49.85, β = 92.78
Total no. of measured intensities	507,669 (18,366)	1,386,043 (69,812)	210,355 (18,117)
Unique reflections	75,200 (3,838)	98,262 (4,890)	15,199 (1,337)
Multiplicity	6.8 (4.8)	14.1 (14.3)	13.8 (13.6)
Mean <i>I</i> / σ (<i>I</i>)	9.2 (1.1)	10.4 (1.2)	10.9 (1.0)
Completeness (%)	98.7 (84.4)	100.0 (100.0)	100.0 (99.9)
<i>R</i> _{merge} [*]	0.104 (1.004)	0.129 (2.029)	0.118 (2.599)
<i>R</i> _{meas} [†]	0.112 (1.126)	0.134 (2.182)	0.122 (2.700)
<i>CC</i> _½ [‡]	0.998 (0.797)	0.999 (0.791)	0.999 (0.436)
Wilson <i>B</i> value (Å ²)	53.5	47.5	52.7
Refinement			
Resolution range (Å)	–	74.21–2.20 (2.26–2.20)	49.84–2.17 (2.23–2.17)
Reflections: working/free [§]	–	93,364/4,855	14,486/687
<i>R</i> _{work} [¶]	–	0.223 (0.402)	0.198 (0.314)
<i>R</i> _{free} [¶]	–	0.251 (0.394)	0.252 (0.342)
Ramachandran plot: favored/ allowed/disallowed (%)	–	99.0/1.0/0.0	99.0/4.0/0.0
R.m.s. bond distance deviation (Å)	–	0.008	0.007
R.m.s. bond angle deviation (°)	–	1.51	1.44
Mean <i>B</i> factor (Å ²)	–	62.6	59.8
PDB accession code	–	8PFC	8PFD

^{*} $R_{\text{merge}} = \frac{\sum_{hkl} \sum_i |I_i(hkl) - \langle I(hkl) \rangle|}{\sum_{hkl} \sum_i I_i(hkl)}$.

[†] $R_{\text{meas}} = \frac{\sum_{hkl} [N(N-1)]^{1/2} \times \sum_i |I_i(hkl) - \langle I(hkl) \rangle|}{\sum_{hkl} \sum_i I_i(hkl)}$, where $I_i(hkl)$ is the *i*th observation of reflection *hkl*, $\langle I(hkl) \rangle$ is the weighted average intensity for all observations *i* of reflection *hkl*, and *N* is the number of observations of reflection *hkl*.

[‡]*CC*_½ is the correlation coefficient between symmetry equivalent intensities from random halves of the dataset.

[§]The dataset was split into “working” and “free” sets consisting of 95 and 5% of the data, respectively. The free set was not used for refinement.

[¶]The R-factors *R*_{work} and *R*_{free} are calculated as follows: $R = \frac{\sum (|F_{\text{obs}} - F_{\text{calc}}|)}{\sum |F_{\text{obs}}|}$, where *F*_{obs} and *F*_{calc} are the observed and calculated structure factor amplitudes, respectively. Values in parentheses are for the outer resolution shell.

and SAP05–Rpn10^{vWA} complexes (rmsd = 0.257 Å) (Fig. 1 *C* and *D*). Moreover, there is no steric hindrance between the ZnF and vWA domains when bound to SAP05. These data provide evidence that SAP05 has a bimodular architecture with opposite loop and sheet surfaces that enable interactions with ZnF of TFs and vWA of Rpn10, thereby acting as a scaffold to link SPL and GATA TFs to Rpn10.

The SAP05 “Loop Surface” Forms Electrostatic Interactions with the ZnF Domain. We further investigated the SAP05 interaction with SPL5^{ZnF}. The crystal structure contains eight copies of the 1:1 complex in the asymmetric unit (ASU), which are closely similar (SI Appendix, Fig. S2). In addition to the two structural Zn²⁺ ions within each SPL5^{ZnF} domain, a further four Zn²⁺ ions are found in the ASU forming crystal contacts (SI Appendix, Fig. S2). These involve E80 from four of the eight SAP05 molecules and H82 and E118 from separate neighbouring copies of SPL5^{ZnF}. The SAP05 loop surface that interacts with ZnF comprises three distinct protruding loops that are separated by β-strands and involves six amino acids of which D66 locates in loop 4, G76, N77, and E80 in loop 5, and R104 and D106 in loop 7 of the SAP05 structure (Figs. 1 *A*, *B*, and *E* and 2*A*). SAP05 binds

the two SPL5 ZnF sites, which are held together by Zn²⁺ ions (Figs. 1*C* and 2*A*) and the complex involve nine connections, with SAP05 amino acids N77 interacting with three amino acids, D106 with two and SAP05 D66, G76, E80, and R104 each with one amino acid of SPL5^{ZnF}, and SAP05 E80 and D106 each forming two interactions with R81 and R121, respectively, of SPL5^{ZnF} (Fig. 2*A* and SI Appendix, Fig. S3*A* and S4*A* and *B*). The majority of the interactions are mediated by hydrogen bonds with some salt bridges and are reinforced by nonbonded contacts (SI Appendix, Fig. S4*A* and Table S1). Distances between the interacting residues range from 2.63 to 3.53 Å (SI Appendix, Fig. S4*B* and *C*). The SAP05–ZnF interaction is dominated by electrostatic interactions of charged and polar residues at the SAP05 loop surface and oppositely charged or polar residues located within α-helices of SPL5^{ZnF} (Fig. 2*B*). To explore the affinity of interaction between SAP05 and SPL5^{ZnF}, we used isothermal titration calorimetry (ITC). Titration of SAP05 into a solution of SPL5^{ZnF} showed an exothermic binding isotherm with a fitted dissociation equilibrium constant (*K*_d) of 0.45 ± 0.06 μM and stoichiometry of 1:1 (Fig. 2*C* and SI Appendix, Fig. S5), and titrating SPL5^{ZnF} into a solution of SAP05 showed a *K*_d of 0.52 ± 0.05 μM (SI Appendix, Fig. S5).

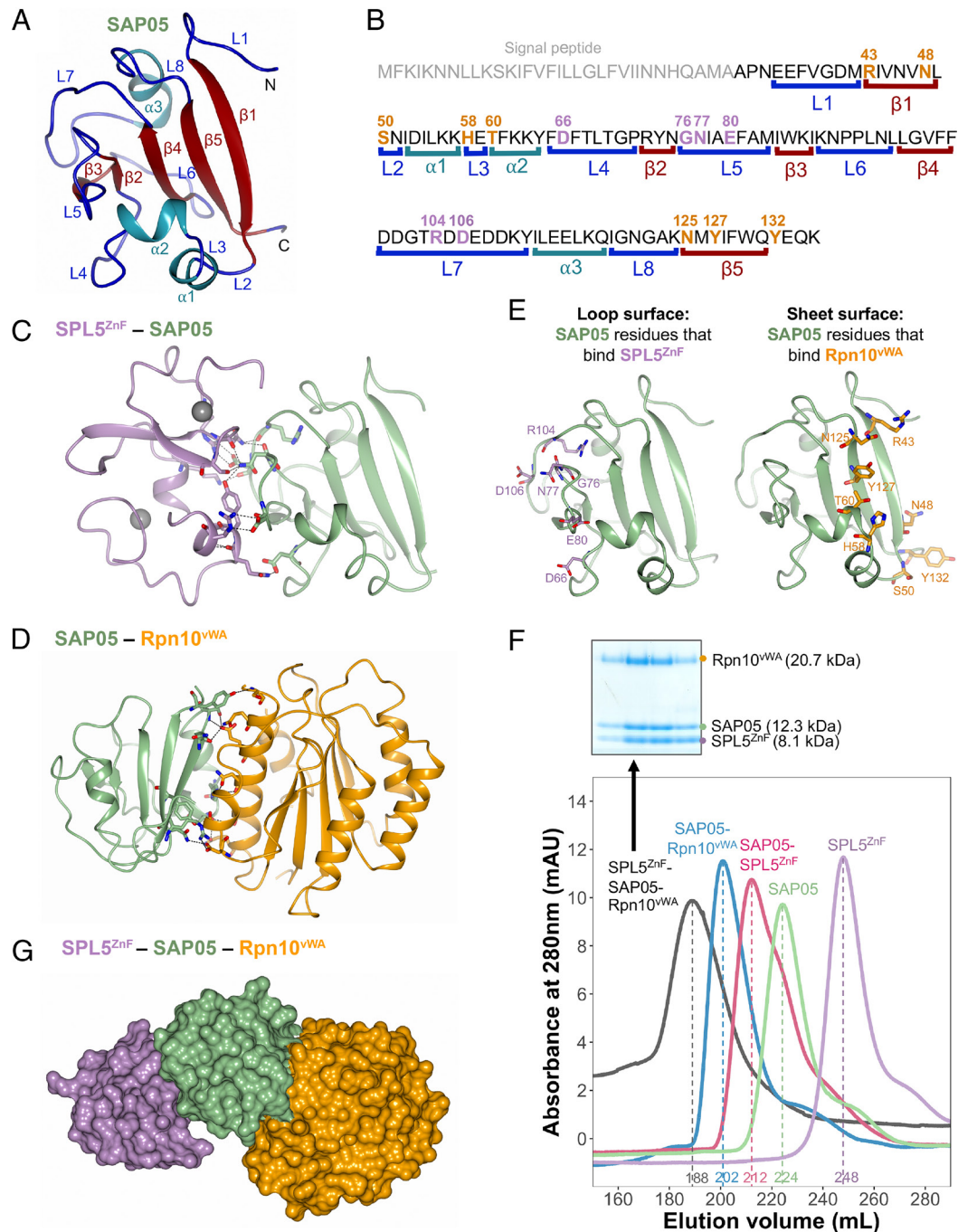


Fig. 1. Crystal structures of SAP5-SPL5^{ZnF} and SAP5-Rpn10^{WVA} complexes revealing the bimodular architecture of SAP5. (A) Cartoon model illustrating the fold of the SAP5 effector. α -helices, β -sheets, and loops are indicated in cyan, red, and blue, respectively. (B) Amino acid sequence of SAP5 highlighting the locations of secondary structures (shown in A, color matched) and SPL5^{ZnF} (purple) and Rpn10^{WVA} interacting residues (orange) (shown in C–F, color-matched). SPL5^{ZnF}, zinc-finger domain of SPL5 transcription factors. Rpn10^{WVA}, von Willebrand factor type A domain of Rpn10 ubiquitin receptor. (C) Crystal structure of the SAP5-SPL5^{ZnF} complex (PDB 8PFC). The Zn²⁺ ions bound to the two ZnF domains are shown in gray. (D) Crystal structure of the SAP5-Rpn10^{WVA} complex (PDB 8PFD). In (C) and (D), the dashed lines indicate the interactions between the residues from both components. (E) Interfaces of SAP5 showing the loop surface (purple) and sheet surface (orange) residues that bind to SPL5^{ZnF} and Rpn10^{WVA}, respectively. (F) Gel filtration chromatograms of SAP5, SPL5^{ZnF}, and Rpn10^{WVA} and ternary complexes of these proteins. The Coomassie-stained protein SDS-PAGE gel shows the presence of the three proteins in the SPL5^{ZnF}-SAP5-Rpn10^{WVA} ternary complex—see *SI Appendix, Fig. S1*, for the other complexes. Elution volumes are indicated at the bottom of each peak with the same colors. (G) Hypothetical ternary structure of SPL5^{ZnF}-SAP5-Rpn10^{WVA} obtained by superimposing the crystal structures of SAP5-SPL5^{ZnF} and SAP5-Rpn10^{WVA} complexes.

We generated 10 structure-guided SAP5 mutants by replacing each residue that forms contacts across the interface with a neutral, similarly charged, or oppositely charged residue (*SI Appendix, Fig. S3A*). The mutants were investigated for their ability to degrade TFs in *Nicotiana benthamiana* leaves using *Agrobacterium*-mediated transient expression assays. SAP5 D66A, G76W, N77R, D106A, and D106R failed to degrade SPL5, though G76W was not detected

in leaves (Fig. 2D). Yeast two-hybrid (Y2H) assays confirmed that these mutants lost the ability to bind SPL TFs, and except for G76W, retained their affinity for Rpn10 (Fig. 2E and *SI Appendix, Fig. S6*). G76W, N77R, D106A, and D106R also retained the ability to bind GATA TFs unlike D66A that lost the ability to bind both SPLs and GATAs (Fig. 2E and *SI Appendix, Fig. S6*). Consistent with these binding activities in Y2H, D66A did not mediate

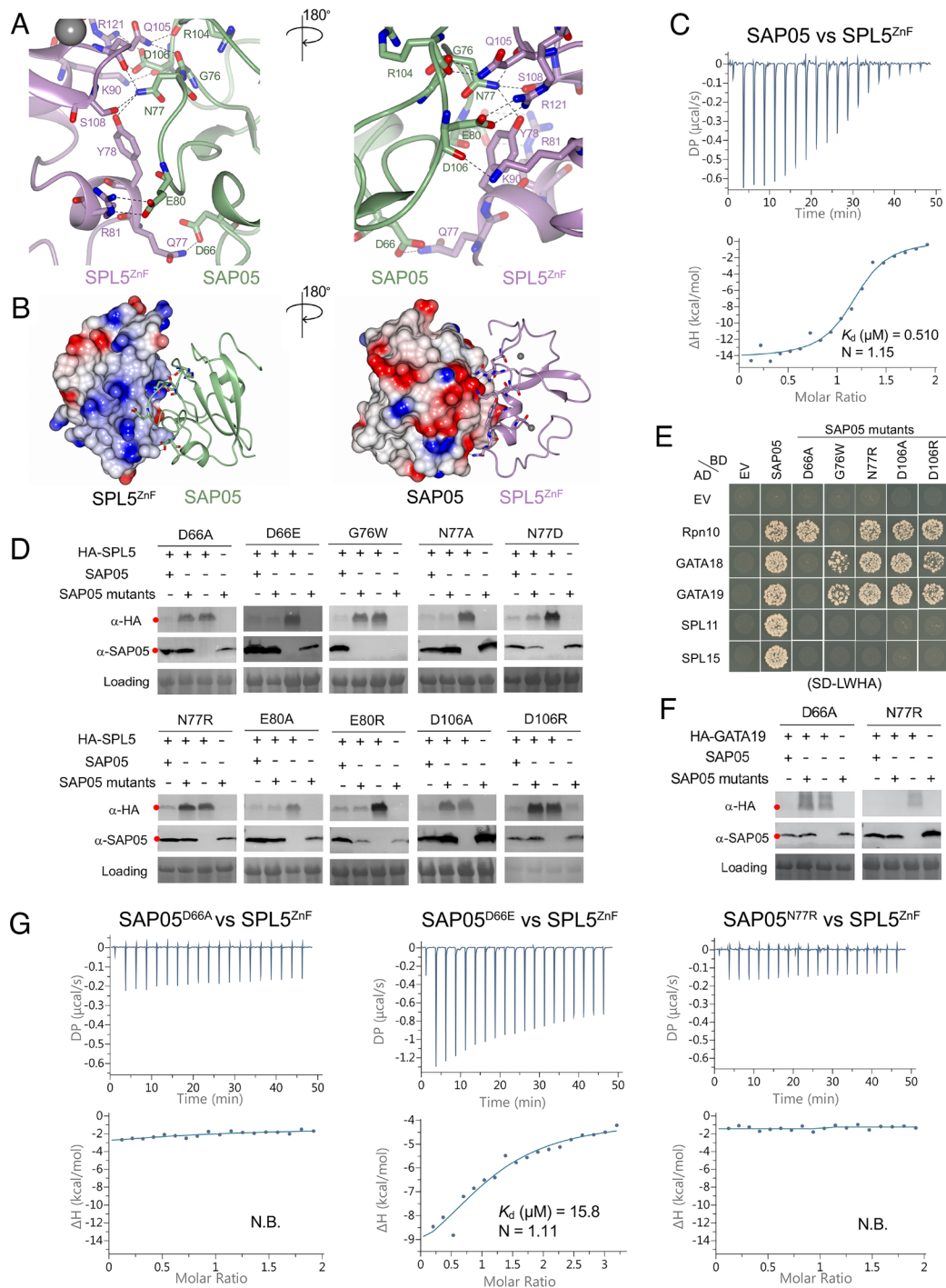


Fig. 2. SAP05 loop surface interacts with SPL5^{ZnF}. (A) Close-up views of SAP05–SPL5^{ZnF} interaction interface from front (Left) and back (Right). The amino acid residues mediating electrostatic interactions are labeled. The Zn²⁺ ions are displayed as gray spheres. (B) Electrostatic potential surface view of SAP05 and SPL5^{ZnF} during complex formation showing that the interacting interface is predominantly electronegative (red) in SAP05 and electropositive (blue) in SPL5^{ZnF}. (C) ITC experiment showing direct physical binding of SAP05 and SPL5^{ZnF}. (D) Western blot analysis of proteasomal degradation of SPL5 in the presence of wild-type or mutant SAP05 in *N. benthamiana* leaves. (E) Yeast two-hybrid (Y2H) assay to test interactions of SAP05 and its mutant versions with *A. thaliana* Rpn10 and GATA and SPL TFs. EV, empty vector control. AD, GAL4-activation domain. BD, GAL4-DNA binding domain. SD-LWHA, quadruple dropout medium lacking leucine, tryptophan, histidine, and adenine. Yeast growth on SD-LW medium is shown in *SI Appendix, Fig. S6A*. (F) Western blot analysis for GATA19 degradation in the presence of SAP05 D66A or N77R mutants in *N. benthamiana* leaves. In (D) and (F), red dots indicate the expected sizes of the transiently expressed proteins. HA, hemagglutinin. Protein loading was visualized using Ponceau S staining. (G) ITC titrations of three SAP05 mutants (D66A, D66E, and N77R) with SPL5^{ZnF}. N.B., not binding. In (C) and (G), the top panels show heat differences upon interaction, and lower panels show integrated heats of injection (•) and the best fit to a single site binding model using MicroCal PEAQ-ITC analysis software. See *SI Appendix, Fig. S5*, for more ITC repeats and thermodynamic parameters.

degradation of GATA19 in leaves whereas N77R did (Fig. 2F). In ITC experiments, SAP05 D66A and N77R mutants did not interact with the ZnF domain of SPL5, whereas SAP05 D66E did, though with lower affinity of a K_d of $17.7 \pm 2.7 \mu\text{M}$ than wild-type SAP05 (Fig. 2 C and G and *SI Appendix, Fig. S5*). Despite this lower

affinity, SAP05 D66E mediates the degradation of SPL5 (Fig. 2D). Therefore, D66, N77, and D106 are required for the SAP05 interactions with the ZnF domain of SPLs. Moreover, D66 is also required for SAP05 interactions with GATA TFs. The finding that SAP05 G76W lost binding to both SPLs and Rpn10 suggests that

this mutant has more profound structural changes, in agreement with its instability in *N. benthamiana* leaves (Fig. 2D). D66 is part of loop 4, N77 of loop 5, and D106 of loop 7 (Figs. 1 A and B and 2A), indicating that all three loop structures of the SAP05 loop surface are involved in binding ZnF of SPLs (Fig. 1 C and E), thereby validating the crystal structure.

Our finding that D66 on one of the loops (loop 4) is involved in binding GATA prompted us to use AlphaFold-Multimer modeling (35) to assess the SAP05–GATA19^{ZnF} complex structure. The AlphaFold model (AFM) of the SAP05 and SPL5^{ZnF} complex and their interactions were consistent with the crystal structure (SI Appendix, Fig. S7A), suggesting a modeling approach could be insightful. We therefore proceeded to predict the SAP05–GATA19^{ZnF} structure using AFM and obtained a high prediction confidence score (SI Appendix, Fig. S7B). In the model, GATA19^{ZnF} interacts with the SAP05 loop surface (SI Appendix, Fig. S7B). Moreover, SAP05 D66, but not N77, is one of the residues involved in the interaction with GATA19 (SI Appendix, Fig. S7C), in agreement with the finding that SAP05 N77R degraded GATA19 in *N. benthamiana* leaves, unlike SAP05 D66A (Fig. 2F). SAP05 F65 of loop 4, E80 of loop 5, and D108 of loop 7 were also predicted to mediate interactions with GATA19 (SI Appendix, Fig. S7C).

Taken together, these data demonstrate that SAP05 interactions with SPL and GATA TFs involve structures of the SAP05 loop surface. Most SAP05 residues involved in binding SPLs and GATAs do not play a role in SAP05 binding of Rpn10 consistent with the bimodular architecture of SAP05.

The SAP05 “Sheet Surface” Forms Polar Interactions with Rpn10^{vWA}. We then further investigated the role of specific residues involved in the SAP05–Rpn10^{vWA} interface. The SAP05 sheet surface comprises two parallel β -strands, β 1 and β 5, as well as two loops separated by an α -helix (Fig. 1 A, B, D, and E). The interaction is mediated by eight SAP05 amino acids, including R43 and N48 located on β 1, S50 on loop 2, H58 on loop 3, T60 on α 2, N125 and Y127 on β 5, and Y132 on the loop following β 5 of SAP05 (Fig. 3A and SI Appendix, Figs. S3B and S8). Each of these residues interacts with one residue of Rpn10^{vWA}, except for T60 that interacts with two residues, and S50 and H58 form two interactions with E31 and N34 of Rpn10^{vWA}, respectively (Fig. 3A and SI Appendix, Fig. S9 A and B). Four of the interactions involve double or single hydrogen bonds and one salt bridge, and other interactions comprise nonbonded contacts (SI Appendix, Fig. S9 A–C and Table S2). Distances between the interacting residues range from 2.48 to 3.76 Å (SI Appendix, Fig. S9 B and C). All Rpn10^{vWA} residues that interact with SAP05 locate on α -helices (Fig. 3A). The Rpn10^{vWA} interaction is largely mediated by polar forces. Thus, the SAP05 sheet surface contains rigid secondary β -sheets and α -helix structures that are held in place by hydrogen bonds within SAP05, as opposed to the ZnF-binding loop surface that involves protruding loop structures that may be more flexible.

We introduced single amino acid mutations in the SAP05 sheet surface by replacing each with neutral, nonpolar or oppositely charged residues generating nine single amino acid SAP05 mutants (SI Appendix, Fig. S3B). All retained the ability to degrade SPL5 in *N. benthamiana* leaves, though some of the SAP05 mutants were not detected in leaves and hence may have high turnover rates (SI Appendix, Fig. S10). However, several SAP05 double mutants and one triple mutant had reduced or no ability to mediate degradation of SPL5 (Fig. 3B), consistent with their loss of binding to Rpn10 in Y2H (Fig. 3C). SAP05 H58A T60W and S50A H58W retained affinity to SPL and GATA TFs (Fig. 3C), indicating that these double mutations have less impacts on the

overall structure of SAP05, compared to the other double mutants that lost affinity to SPLs and the triple mutant that did not bind any of the targets. These data indicate that multiple SAP05 residues mediate interactions with vWA, thereby validating the crystal structure.

In ITC experiments, the interaction of the SAP05–Rpn10^{vWA} complex with SPL5^{ZnF} has a K_d of $0.65 \pm 0.04 \mu\text{M}$ and stoichiometry of 1:1 (Fig. 3D and SI Appendix, Fig. S5), which is similar to that of SAP05 alone with SPL5^{ZnF} (Fig. 2C and SI Appendix, Fig. S5). This indicates that vWA-bound SAP05 does not undergo a major change in configuration compared to SAP05 alone, in agreement with crystal structure data (Fig. 1 C and D). However, the K_d of the SAP05 H58A T60W interaction with SPL5^{ZnF} is $3.60 \pm 0.81 \mu\text{M}$ (Fig. 3E and SI Appendix, Fig. S5), indicating that the H58A T60W mutations impact the efficiency of SAP05 to bind SPL5^{ZnF}. Nonetheless, SAP05 H58A T60W retains affinity to SPL and GATA TFs and mediates the degradation of SPL5 (Fig. 3 B and C), in line with the bimodular architecture of SAP05.

Conservation Analyses of SAP05 Residues Involved in SAP05–ZnF and SAP05–vWA Interaction Reveal Dynamic Evolutionary Patterns.

We previously identified SAP05 homologs in phytoplasm, including examples that bind both SPLs and GATAs and ones that bind only SPLs or only GATAs (5). SAP05 amino acids that interact with SPL5 and vWA are conserved among all or most SAP05 homologs, including D66 that mediates binding with SPL and GATA TFs (SI Appendix, Fig. S11A). The SAP05 homologs that exclusively bind SPLs (PnWBa, WBDLa, and P. mali) and that bind only GATAs (PnWBb and WBDLb) exhibited the greatest sequence variation in their interacting residues compared to other SAP05 homologs (SI Appendix, Fig. S11A). We noticed that regions corresponding to SAP05 residues 67 to 73 (FTLTGPR) that form loop 4 and connect to β 2 in SAP05_AYWB (Fig. 1 A and B) were different in sequence among the SPL versus GATA-binding SAP05 homologs (SI Appendix, Fig. S11A). Loop 4 starts with the conserved F65 and D66 amino acids (Fig. 1 A and B and SI Appendix, Fig. S11A). Given our finding herein that D66 is essential for both SPL and GATA binding and degradation (Fig. 2), we investigated whether loop 4 is involved in determining SAP05-binding specificity for SPLs and GATAs. Swapping corresponding loop 4 sequences from SAP05 homologs PnWBa and WBDLa to PnWBb and WBDLb resulted in gain of SPL binding, and conversely, swapping these from PnWBb and WBDLb to PnWBa and WBDLa resulted in gain of GATA binding (SI Appendix, Fig. S11 B and C). Therefore, loop 4 contributes to SAP05 binding specificity to SPLs and GATAs.

Next, we determined in how far interacting residues are conserved among the ZnF domains of SPL TFs. The zinc-binding domain of SPL proteins contains two zinc-binding sites formed by eight conserved Cys or His residues (31). SAP05-binding residues locate in both ZnF domains and the majority of these are conserved among the SPL TFs (SI Appendix, Fig. S12). However, SAP05 D66 interacts with Q77 in SPL5, and this amino acid is not conserved (SI Appendix, Fig. S12). Given the importance of SAP05 D66 in mediating interactions with both SPL and GATAs, we examined the electrostatic surface in the position of SAP05 D66. In wild-type SAP05, the surface area around D66 is electronegative (SI Appendix, Fig. S13 A and C), while the electronegativity of this surface area is reduced in the SAP05 D66A mutant that lost interaction with SPL5 and GATA19 (SI Appendix, Fig. S13 B and D). Furthermore, the SAP05 D66E mutant, which is equally charged with negative residue glutamic acid, still binds and degrades SPL5 in planta (Fig. 2 D and G). Taken together, these results indicate that the electronegative surface potential

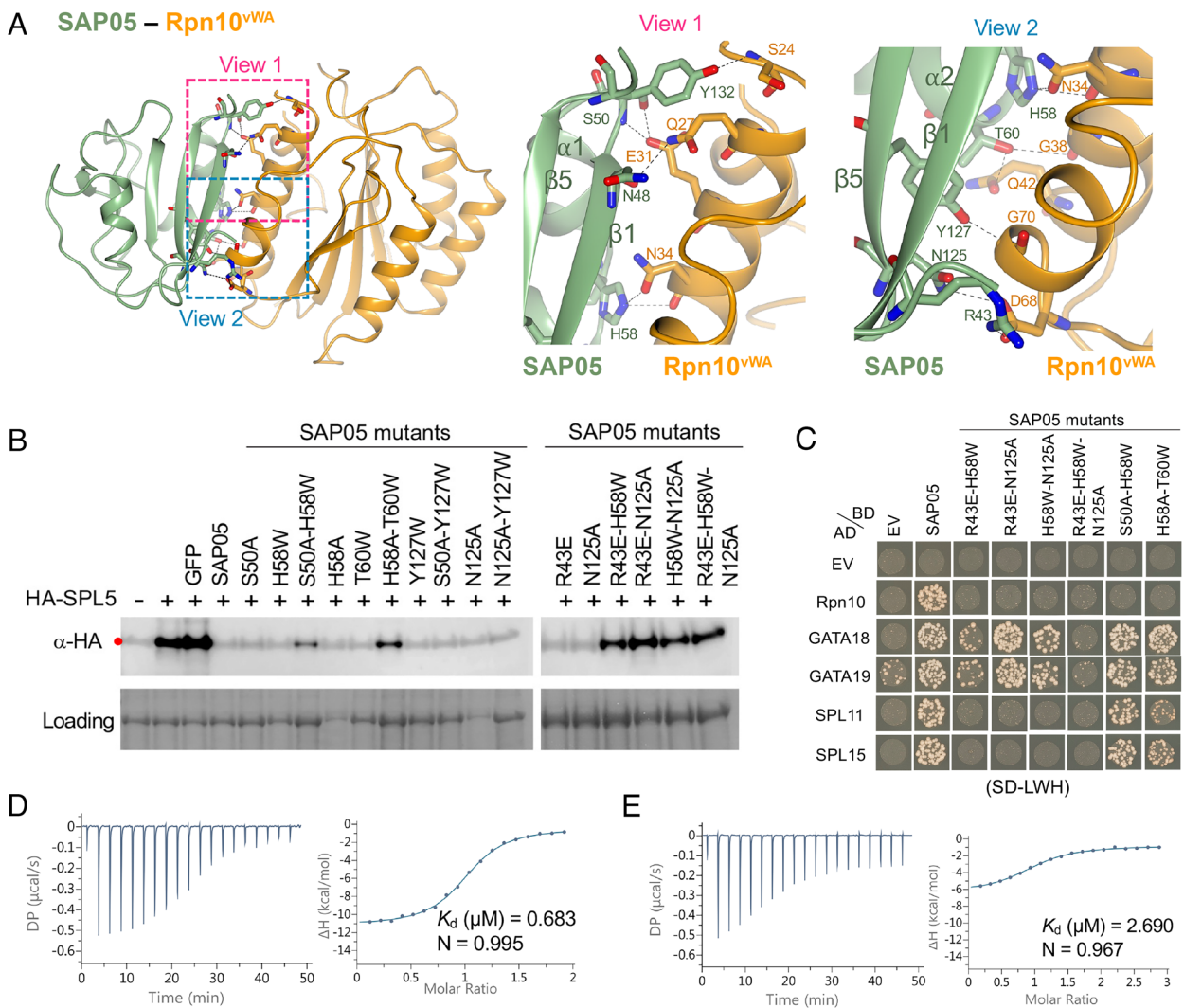


Fig. 3. SAP05 β -sheet surface binds to Rpn10^{vWA}. (A) Close-up views of SAP05–Rpn10^{vWA} interaction interface showing the residues involved in complex formation. *Left*, overview of the interacting interface with two dashed squares displaying the areas for enlarged view. *Middle*, the enlarged view 1 of the top part in the interface. *Right*, the enlarged view 2 of the lower part in the interface. (B) Western blot analysis for SPL5 degradation with SAP05 wild-type and mutants in *A. thaliana* protoplasts. GFP, green fluorescent protein control. HA, hemagglutinin. Protein loading was visualized using Amido Black staining. (C) Y2H assay to test interactions of SAP05 and its mutants with *A. thaliana* Rpn10 and GATA and SPL TFs. EV, empty vector control. AD, GAL4-activation domain. BD, GAL4-DNA binding domain. SD-LWH, triple dropout medium lacking leucine, tryptophan, and histidine. See *SI Appendix, Fig. S6B*, for yeast growth on SD-LW medium. (D and E) ITC titrations of the SAP05–Rpn10^{vWA} complex with SPL5^{2nf} (D) and SAP05^{H58A-T60W} with SPL5^{2nf} (E). Left panels show heat differences upon interaction and right panels show integrated heats of injection (+) and the best fit to a single site binding model using MicroCal PEAQ-ITC analysis software. See *SI Appendix, Fig. S5*, for more ITC repeats and thermodynamic parameters.

contributed by D66 is an important factor for binding SPL and GATA TFs.

Among the SAP05 residues that bind vWA, particularly H58, in combination with S50 or T60, have essential roles (Fig. 3). These locate in loop 2 and loop 3 that connect $\alpha 1$ and $\alpha 2$ in the SAP05 structure (Fig. 1 *A* and *B*). SAP05 H58 is conserved among the majority of SAP05 homologs (*SI Appendix, Fig. S7A*) and interacts with N34 that is conserved in vWA domains of most Rpn10 homologs (*SI Appendix, Fig. S14*). SAP05 S50 interacts with *A. thaliana* vWA E31 that is also an acidic amino (D) in other vWA sequences, and SAP05 T60 with G38 and Q42 that are conserved among plant vWA (*SI Appendix, Fig. S14*). The four amino acids locate in the first α -helix (positions 25 to 43) at the N terminus of *A. thaliana* vWA (Fig. 4 and *SI Appendix, Fig. S14*).

We previously reported that SAP05 does not interact with insect and human Rpn10 (the latter is also known as PSMD4) and that replacing AtvWA G38 and A39 with human H38 and S39, respectively, prevented SAP05 binding (5). Multiple sequence alignment

of plant and animal vWA domains showed high conservation with a few amino acid differences (*SI Appendix, Fig. S14*). Structural superimposition of SAP05 interactions with vWA domains of plant Rpn10 and PSMD4 revealed that SAP05 loop 3 clashes with H38 of PSMD4 precluding a SAP05–PSMD4 interaction (Fig. 4). Similarly, Q38 of vWA of yeast Rpn10 clashes with loop 3 of SAP05 precluding SAP05 from binding yeast Rpn10 (Fig. 4). This corroborates data presented herein that H58 of the SAP05 loop 3 region plays an essential role in the SAP05 interaction with *A. thaliana* vWA.

Positioning of the SAP05 Complex on the 26S Proteasome Points to a TPD Mechanism. Rpn10 is positioned in the 19S RP where it forms an important component in the interface of the lid and base structure (36). The cryo-EM structure of the spinach (*Spinacia oleracea*) 26S proteasome was recently resolved (32). The vWA residues that interact with 26S proteasome are conserved in *S. oleracea* and *A. thaliana* Rpn10 homologs (*SI Appendix, Fig. S15*). The structural superimposition of SAP05–Rpn10^{vWA} complex onto the spinach 26S

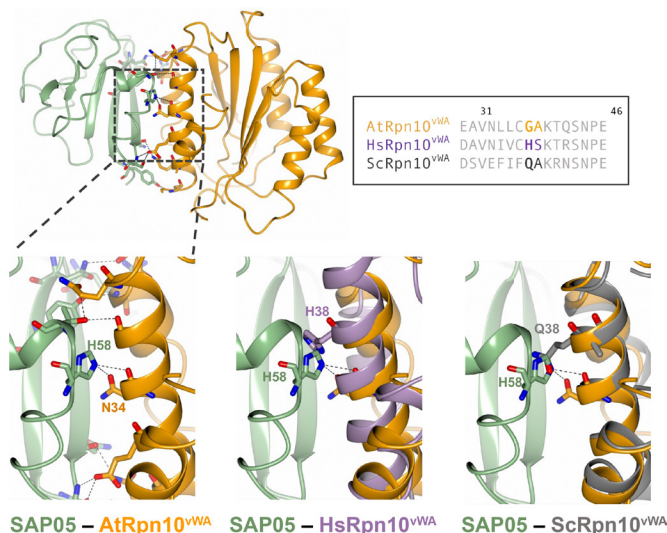


Fig. 4. Steric clash at the SAP05 loop 3 region prevents SAP05 binding to human and yeast vWA domains. The SAP05–AtRpn10^{vWA} complex structure was aligned with the vWA domain structures of human Rpn10 (PSMD4, PDB 6MSD) and yeast (*S. cerevisiae*) Rpn10 (PDB5LN1) to compare their configurations. The dashed squared box on the top left shows the position of loop 3. Box on the top right, sequence alignment of vWA sequences from *A. thaliana* Rpn10 (Uniprot ID: P55034); HsRpn10, *H. sapiens* Rpn10 (Uniprot ID: Q5VWC4); ScRpn10, *S. cerevisiae* Rpn10 (Uniprot ID: P38886).

proteasome did not reveal obvious steric clashes with proteasome components (Fig. 5A). Notably, SAP05 interacts with two parallel α -helices that locate on a region of vWA that does not interact with the 19S subunit (Fig. 5B). This suggests that SAP05 has minimal disadvantageous effects on Rpn10 interactions with the 19S RP. However, the SPL5^{ZnF} of the ternary structure sterically clashes with two α -helices that protrude from the 26S proteasome (*SI Appendix, Fig. S16A*). We found that these helices are derived from the flexible N-terminal coiled-coil (CC) domains of the spinach homologs of *A. thaliana* Rpt4 and Rpt5 (*SI Appendix, Fig. S16A*), which are part of the 6 AAA+ ATPase (Rpt1-6) subunit ring that sits on top of the 20S CP. The CC domains of these Rpt proteins play an important role in physically connecting substrate recruitment and processing (37) and may therefore be involved in SPL5^{ZnF} binding and degradation. We propose that interaction of SPL5 with the CC dimer may induce the degradation of the transcription factor.

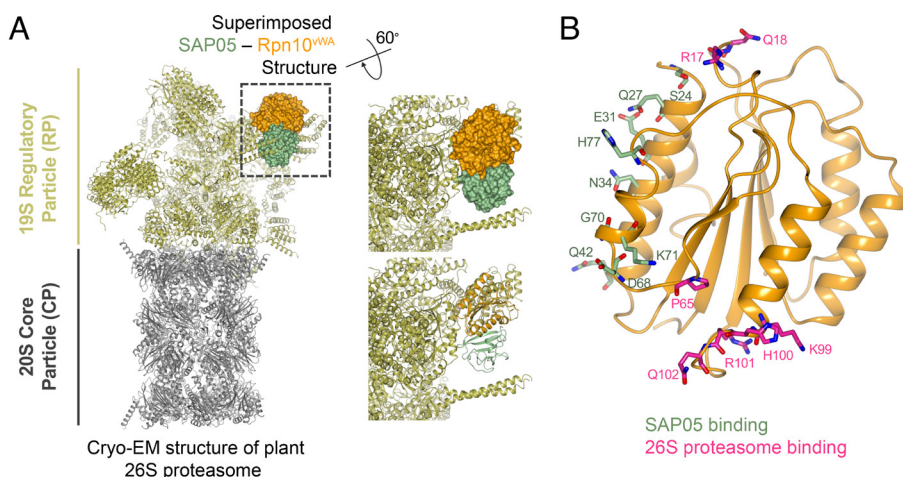


Fig. 5. SAP05 interaction with the Rpn10^{vWA} domain has no hindrance on the plant 26S proteasome. (A) Structural superimposition of SAP05–Rpn10^{vWA} on the spinach 26S proteasome (PDB 7QVE and PDB 8AMZ). The dashed square box shows the parts with superimposition and is enlarged to show the surface (Right Top) and cartoon (Right Bottom) view of the SAP05–Rpn10^{vWA} complex. (B) Position of Rpn10^{vWA} residues interacting with SAP05 (green) and subunits of the 26S proteasome (pink).

Discussion

The crystal structure data reported herein demonstrate that the 12.3-kDa bacterial effector SAP05 has a globular structure with an internal β -sheet core and interconnecting loops and α -helices. One interaction surface is dominated by rigid β -strands (sheet surface) and the opposite surface by loop structures (loop surface) that may be more flexible in their configurations. The rigid sheet surface binds the vWA domain of plant Rpn10 and cannot bind vWA domains of Rpn10 homologs of several organisms other than plants, even though the vWA domains are highly conserved among Rpn10 homologs. The flexible loop surface is however capable of binding multiple transcription factors of the distinct SPL and GATA TF families via their zinc-finger domains. Therefore, SAP05 appears to have an optimal configuration to act as a molecular bridge capable of connecting a conserved proteasome component to multiple members of two TF families.

Rpn10^{vWA} has an important function as its deletion causes lethality or severe growth deficiencies in plants, vertebrates, and human cell lines (38–40). In *rpn10* null mutants, deficiencies may be restored upon addition of Rpn10^{vWA} and RAD23, and Rpn10 and RAD23 act redundantly (41, 42). Like Rpn10, RAD23 is a reversible component of the 26S proteasome and binds ubiquitinated substrates (41). Intriguingly, the phytoplasma SAP54/phylogen family of effectors hijack RAD23 and mediate plant proteins, the MADS-box TFs for degradation, leading to plant developmental changes (29, 30). SAP54 bind the RAD23 ubiquitin-associated (UBA) that are shown to noncovalently bind ubiquitin moieties of ubiquitinated substrates (26, 43). Therefore, at least two distinct phytoplasma effector families mediate degradation of plant TFs in ubiquitin-independent manner using reversible components of the 19S RP.

The vWA domain locates at the N terminus of Rpn10, followed by a flexible region connecting single-helix ubiquitin interaction motifs (UIMs) that bind ubiquitin chains in the C-terminal half of Rpn10 (44, 45). Due to the flexibility of the C-terminal half of Rpn10, only the vWA domain is visible in cryo-EM structures of 26S proteasomes and locates in a central location of the 19S RP, at the interface of its base and lid (46). There is no evidence that SAP05 interferes with 26S proteasome activity (5) and structural information generated herein shows that SAP05 binds to a region of vWA that does not interact with components of the 19S RP. Therefore, SAP05 appears to have evolved to

optimally bind plant Rpn10, which is positioned in a central location of the 19S RP.

Our findings indicate that the placement of the SAP05 complex on the 26S proteasome suggests a TPD mechanism. While the SAP05–Rpn10^{vWA} complex does not appear to cause significant steric hindrance, the SPL5^{ZnF} within the ternary structure appears to clash sterically with the α -helices of Rpt4 and Rpt5, as evidenced in the structural model of the spinach 26S proteasome (32). The coiled-coil (CC) domains of these two Rpt proteins, along with the domains of four others, dimerize to create three CCs (Rpt1/2, Rpt6/3, and Rpt4/5 CCs). These CCs play a vital role in 26S proteasome activity by physically linking substrate recruitment and processing to the unfolding machinery, ultimately leading to substrate degradation (47). Furthermore, conformational changes within the CCs are essential for transitioning the Rpt1-6 ATPase ring between resting and active states (37), the latter of which involves a widening of the central pore to allow substrate entry into the core of the 20S CP (47). The Rpt4/5 CC also binds to Rpn10 upon substrate binding (47). As such, when the ternary complex is accommodated on the 26S proteasome, the interaction of SPL5 with the CC dimer could potentially instigate the switch of the proteasome to the active state, leading to the degradation of the transcription factor.

The ternary structure was modeled on the spinach 26S proteasome recognition state structure. However, the 26S proteasome changes configuration during the processing of substrates. To investigate how the SAP05 ternary complex may be positioned on the different configurations of the 26S proteasome, we used the structures of the human 26S proteasome substrate recognition (PDB 6MSD), deubiquitination (PDB 6MSE) and translocation initiation (PDB 6MSH) states that have been resolved (48) for modeling. The CC domains of Rpt4 and Rpt5 also clash with SPL5^{ZnF} of the superimposed SAP05 ternary complex on the substrate recognition and deubiquitination states, whereas they clash with SAP05 in the translocation initiation state of the human 26S proteasome (*SI Appendix, Fig. S16B*). However, the Rpt subunits are known to undergo conformational changes to hold the substrate in place (37, 49). Therefore, it remains to be determined where the CC domains locate in the presence of the SAP05 ternary complex. SAP05 may also disengage once SPL5 is starting its translocation into the central pore for degradation. Another consideration is that full-length SPL5 is likely to cause more clashes with proteasome components than SPL5^{ZnF}. However, AlphaFold2 predictions show that the regions that directly flank the ZnF domain at both ends of the SPL5 protein are highly unstructured (*SI Appendix, Fig. S17*), indicating that these regions might be inherently flexible thereby enabling SPL5 accommodation on the proteasome.

We investigated the importance of residues mediating the SAP05–SPL5^{ZnF} and SAP05–Rpn10^{vWA} interactions. We found that mutations of single amino acids in SAP05 disrupted the SAP05–SPL5^{ZnF} interaction. Some mutations in SAP05 had little impact on SPL5 stability. These include N77A and N77D. However, another mutation involving the same amino acid, such as N77R, abolished the ability of SAP05 to bind SPL5^{ZnF} and mediate the degradation of SPL5. An explanation is that neutral (A) and negatively charged (D) amino acids at the N77 location do not affect SPL5 binding, whereas a positively charged amino acid (R) does. This agrees with our observation that an electronegative surface of SAP05 is primarily responsible for binding the TFs. SAP05 mutant D66A is impaired in the degradation of both SPL5 and GATA19, showing a potential to be further engineered for a useful tool to degrade any protein without inducing plant developmental changes.

In contrast, multiple amino acid mutations are needed to impair SAP05 interaction with Rpn10^{vWA}. Even in the SAP05 H58A T60W and S50A H58W double mutants, the ability to mediate degradation has not fully disappeared. This suggests that the SAP05–Rpn10^{vWA} interaction is robust. It is striking that SAP05 itself is not degraded, and is highly stable in plant cells, despite its association with the 26S proteasome and its function in degrading substrates that it directly interacts with. However, the study herein revealed that SAP05 derivatives with mutations in the SAP05–Rpn10^{vWA} interaction surface are often unstable in plant cells. A possible explanation of these results is that, compared to wild-type SAP05, the SAP05 mutants have weaker interactions with vWA and this leads to the SAP05 mutant being dragged down along with ZnF when the latter is pulled into the core of the 20S CP. We were unable to test this with ITC experiments because purified vWA on its own (without SAP05) forms aggregates. Nonetheless, results so far suggest that SAP05 stability is linked to its association with Rpn10. During the revision of this manuscript, other SAP05 crystal structures were resolved, including that of the SAP05 homologue of Onion Yellow phytoplasma in complex with Rpn10^{vWA} (50), revealing similar structures as reported herein.

In summary, SAP05 displayed no notable structural similarity to any experimentally confirmed structures in the Protein Data Bank (PDB). We suggest that this effector protein possesses a molecular architecture that enables it to connect host proteins to the Ubiquitin Proteasome System (UPS), thereby circumventing the canonical targeted protein degradation pathway. Impaired functioning of the UPS is linked with a multitude of diseases. However, given the pivotal role of the UPS in orchestrating an array of cellular processes, the SAP05 molecular system presents opportunities for the development of innovative therapeutics. Notably, Rpn10 has been recognized as a potential therapeutic target (51). Furthermore, the 26S proteasome has been leveraged to create therapeutics such as PROTACs (PROteolysis-TArgeting Chimeras), which are small molecules that recruit E3 ligases for ubiquitination of substrates marked for degradation (52). Several PROTACs and similar systems have shown promising results and are currently advancing through clinical trials. However, their reliance on recruiting E3 ligases has led to challenges associated with side effects and resistance. Since SAP05 does not hamper the ability of the 26S proteasome to degrade substrates, this effector emerges as a prime candidate for engineering a type of degraders that operate independently of E3 ligases. The structural work presented in this study provides a springboard for bioengineering a class of degraders that do not depend on E3 ligases.

Materials and Methods

Gene Cloning for Crystallization. For the purpose of crystallization of the SAP05–SPL5^{ZnF} and SAP05–Rpn10^{vWA} complexes, gene fragments corresponding to SAP05 (Ala33–Lys135) and ZnF domain of SPL5 (Ser60–Leu127) were separately subcloned to various pOPINF vectors, and SAP05 (Ala33–Lys135) and Rpn10^{vWA} (Val2–Gly193) were co-subcloned to pOPINA vectors using In-fusion cloning strategy (53, 54) as described in *SI Appendix, Materials and Methods*.

SAP05 Mutation Generation. SAP05 mutants were generated by overlap PCR (55) or directly synthesized using gBlock from Integrated DNA Technologies company (IDT). Mutations used for different assays were codon optimized and cloned to different vectors.

Protein Expression and Purification. Plasmids expressing the SAP05, SPL5^{ZnF}, SAP05, and Rpn10^{vWA} were expressed in *E. coli* BL21 (DE3) competent cells. Proteins were purified via IMAC followed by gel filtration. Purified proteins were pooled and concentrated to 15 mg/mL for crystallization studies. Detailed procedures are provided in *SI Appendix, Materials and Methods*.

37. A. Snoberger, E. J. Brettrager, D. M. Smith, Conformational switching in the coiled-coil domains of a proteasomal ATPase regulates substrate processing. *Nat. Commun.* **9**, 2374 (2018).
38. A. S. Fatimababy *et al.*, Cross-species divergence of the major recognition pathways of ubiquitylated substrates for ubiquitin/26S proteasome-mediated proteolysis. *FEBS J.* **277**, 796–816 (2010).
39. J. Hamazaki *et al.*, Rpn10-mediated degradation of ubiquitinated proteins is essential for mouse development. *Mol. Cell Biol.* **27**, 6629–6638 (2007).
40. N. Rani, A. Aichem, G. Schmidtke, S. G. Kreft, M. Groettrup, FAT10 and NUB1L bind to the VWA domain of Rpn10 and Rpn1 to enable proteasome-mediated proteolysis. *Nat. Commun.* **3**, 749 (2012).
41. S. Elsasser, D. Chandler-Militello, B. Müller, J. Hanna, D. Finley, Rad23 and Rpn10 serve as alternative ubiquitin receptors for the proteasome. *J. Biol. Chem.* **279**, 26817–26822 (2004).
42. R. Verma, R. Oania, J. Graumann, R. J. Deshaies, Multiubiquitin chain receptors define a layer of substrate selectivity in the ubiquitin-proteasome system. *Cell* **118**, 99–110 (2004).
43. L. Chen, U. Shinde, T. G. Ortolan, K. Madura, Ubiquitin-associated (UBA) domains in Rad23 bind ubiquitin and promote inhibition of multi-ubiquitin chain assembly. *EMBO Rep.* **2**, 933–938 (2001).
44. E. Sakata *et al.*, Localization of the proteasomal ubiquitin receptors Rpn10 and Rpn13 by electron cryomicroscopy. *Proc. Natl. Acad. Sci. U.S.A.* **109**, 1479–1484 (2012).
45. Q. Wang, P. Young, K. J. Walters, Structure of S5a bound to monoubiquitin provides a model for polyubiquitin recognition. *J. Mol. Biol.* **348**, 727–739 (2005).
46. X. Chen *et al.*, Cryo-EM reveals unanchored M1-ubiquitin chain binding at hRpn11 of the 26S proteasome. *Structure* **28**, 1206–1217.e1204 (2020).
47. M. E. Matyskiela, G. C. Lander, A. Martin, Conformational switching of the 26S proteasome enables substrate degradation. *Nat. Struct. Mol. Biol.* **20**, 781–788 (2013).
48. Y. Dong *et al.*, Cryo-EM structures and dynamics of substrate-engaged human 26S proteasome. *Nature* **565**, 49–55 (2019).
49. P. Śledź *et al.*, Structure of the 26S proteasome with ATP- γ S bound provides insights into the mechanism of nucleotide-dependent substrate translocation. *Proc. Natl. Acad. Sci. U.S.A.* **110**, 7264–7269 (2013).
50. L. Zhang, Y. Du, Q. Zheng, Structure basis of the phytoplasma effector SAP05 recognition specificities to plant Rpn10 in ubiquitin-independent protein degradation. bioRxiv [Preprint] (2023). <https://doi.org/10.1101/2023.08.24.554544> (Accessed 13 September 2023).
51. T. Du *et al.*, Ubiquitin receptor PSMD4/Rpn10 is a novel therapeutic target in multiple myeloma. *Blood* **141**, 2599–2614 (2023).
52. X. Lu *et al.*, Structure-guided bifunctional molecules hit a DEUBAD-lacking hRpn13 species upregulated in multiple myeloma. *Nat. Commun.* **12**, 7318 (2021).
53. R. M. Benoit, R. N. Wilhelm, D. Scherer-Becker, C. Ostermeier, An improved method for fast, robust, and seamless integration of DNA fragments into multiple plasmids. *Protein Expr. Purif.* **45**, 66–71 (2006).
54. L. E. Bird *et al.*, Application of in-fusion™ cloning for the parallel construction of *E. coli* expression vectors. *Methods Mol. Biol.* **1116**, 209–234 (2014).
55. M. D. Nelson, D. H. Fitch, Overlap extension PCR: An efficient method for transgene construction. *Methods Mol. Biol.* **772**, 459–470 (2011).
56. A. Dereeper *et al.*, Phylogeny.fr: Robust phylogenetic analysis for the non-specialist. *Nucleic Acids Res.* **36**, W465–W469 (2008).
57. K. Tamura, G. Stecher, S. Kumar, MEGA11: Molecular evolutionary genetics analysis version 11. *Mol. Biol. Evol.* **38**, 3022–3027 (2021).
58. J. Jumper *et al.*, Highly accurate protein structure prediction with AlphaFold. *Nature* **596**, 583–589 (2021).
59. S. McNicholas, E. Potterton, K. S. Wilson, M. E. Noble, Presenting your structures: The CCP4mg molecular-graphics software. *Acta Crystallogr. D Biol. Crystallogr.* **67**, 386–394 (2011).
60. R. A. Laskowski *et al.*, PDBsum: Structural summaries of PDB entries. *Protein Sci.* **27**, 129–134 (2018).
61. W. Huang *et al.*, Crystal structure of binary complex between Aster yellows witches'-broom phytoplasma effector SAP05 and the zinc finger domain of SPL5 from *Arabidopsis thaliana*. Protein Data Bank. <https://doi.org/10.2210/pdb8pfc/pdb>. Deposited 15 June 2023.
62. W. Huang *et al.*, Crystal structure of binary complex between Aster yellows witches'-broom phytoplasma effector SAP05 and the von Willebrand Factor Type A domain of the proteasomal ubiquitin receptor Rpn10 from *Arabidopsis thaliana*. Protein Data Bank. <https://doi.org/10.2210/pdb8pfd/pdb>. Deposited 15 June 2023.